An Experimental and Multiphysics Simulations Study of *Clostridium carboxidivorans* sp. 624 for Acid and Alcohol Production in CO_2/H_2

Yong Wei Tiong[a, b, 1, *], Ashriel Yong[a, b, 1], Anjaiah Nalaparaju[c, 1, *], Hoang-Huy Nguyen[c, 1], Li Quan Koh[a], Roong Jien Wong[a], Ron Tau Yee Lim[a], Dave Siak-Wei Ow[d], Jia Zhang[c], Van Bo Nguyen[c], Fong Tian Wong[a, b, e, *], Yee Hwee Lim[a, b, f, *]

[a]Institute of Sustainability for Chemicals, Energy and Environment (ISCE[2]), Agency for Science, Technology and Research (A*STAR), 1 Pesek Road, Jurong Island, Singapore 627833, Republic of Singapore

[b]Singapore Integrative Biosystems and Engineering Research (SIBER), Agency for Science, Technology and Research (A*STAR), 20 Biopolis Way, #08-01 Centros, Singapore 138668, Republic of Singapore

[c]Institute of High Performance Computing (IHPC), Agency for Science, Technology and Research (A*STAR), 1 Fusionopolis Way, #16-16 Connexis North, Singapore 138632, Republic of Singapore

[d]Bioprocessing Technology Institute (BTI), Agency for Science, Technology and Research (A*STAR), 20 Biopolis Way, #06-01 Centros, Singapore 138668, Republic of Singapore

[e]Institute of Molecular and Cell Biology (IMCB), Agency for Science, Technology and Research (A*STAR), 61 Biopolis Drive, #07-06 Proteos, Singapore 138673, Republic of Singapore

[f]Synthetic Biology Translational Research Program, Yong Loo Lin School of Medicine, National University of Singapore, 10 Medical Drive, Singapore 117597, Republic of Singapore

[1]These authors contributed equally to this work.

*Co-corresponding authors:

Institute of Sustainability for Chemicals, Energy and Environment (ISCE[2]), Agency for Science, Technology and Research (A*STAR), 1 Pesek Road, Jurong Island, Singapore 627833, Republic of Singapore.

Email address:

lim_yee_hwee@isce2.a-star.edu.sg (Yee Hwee Lim),

wongft@imcb.a-star.edu.sg (Fong Tian Wong),

Tiong_Yong_Wei@isce2.a-star.edu.sg (Yong Wei Tiong)

Institute of High Performance Computing (IHPC), Agency for Science, Technology and Research (A*STAR), 1 Fusionopolis Way, #16-16 Connexis North, Singapore, 138632 Republic of Singapore.

Email address: Anjaiah_Nalaparaju@ihpc.a-star.edu.sg (Anjaiah Nalaparaju)

Abstract

Biotechnological advancements in carbon utilization, particularly CO_2 gas fermentation, present a sustainable alternative to energy-intensive chemical catalysis. *Clostridium carboxidivorans* sp. 624, a clostridial acetogen, employs the Wood-Ljungdahl pathway to fix CO_2, producing valuable acids and alcohols. In this study, we systematically investigate the metabolic dynamics of CO_2/H_2 fermentation, focusing on optimizing temperature and media conditions to enhance yield. Notably, batch fermentation at 25°C achieved the highest reported acetate concentration of 4.38 g/L, with butyrate and hexanoate detected at lower yields. To further optimize fermentation performance, we examined the impact of the liquid-to-gas volume ratio (V_L/V_G) on product distribution. Acetate remained dominant, while V_L/V_G = 4 enhanced longer-chain acid production, due to improved gas solubility and substrate bioavailability. The enriched liquid phase at V_L/V_G = 4 also drove higher total acid (5.341 g/L) and alcohol (0.411 g/L) production. Moreover, the acid-to-alcohol ratio was 13 for V_L/V_G = 4, promoting alcohol conversion, while a higher ratio of 18 for V_L/V_G = 1 maintained an acetogenic profile. To complement the experimental insights, a kinetic model coupled with 3D computational fluid dynamics simulations was developed to elucidate spatial inhomogeneity and its impact on reaction kinetics. This comparative analysis identified key optimized parameters, including maximum reaction rates, half-saturation concentrations, and inhibition rates, which serve as critical guidelines for enhancing fermentation performance. By leveraging real-time computational modelling to refine bioreactor design, this approach facilitates the transition toward scalable CO_2 bioprocessing. These findings advance of sustainable chemical manufacturing, reinforcing CO_2 bioconversion as a strategy for carbon-negative biotechnology.

Keywords: *Clostridium carboxidivorans*; CO_2 fermentation; Process optimization; Acid and alcohol selectivity; Kinetic modelling; Computational fluid dynamics

1. Introduction

Atmospheric CO_2 levels have risen from 277 ppm in 1750 to 421 ppm by 2022, driven by fossil fuel combustion (Raganati and Ammendola, 2024). In 2021, global CO_2 emissions surged 6% to 36.3 gigatonnes as economies rebounded post-COVID-19 (Dziejarski et al., 2023). In response, the Paris Agreement targets 50-100% emissions reduction by 2030 and beyond (Lau et al., 2021; Ulpiani et al., 2023). In light of this, biotechnological CO_2 utilization is gaining attention for its sustainability over chemical catalysis (Liew et al., 2016), using microorganisms to convert CO_2 into valuable bio-based products, advancing a circular economy (Ricci et al., 2021).

One prominent example is anaerobic CO_2 gas fermentation, where clostridial acetogens use the Wood-Ljungdahl pathway (WLP), also known as the reductive acetyl-CoA pathway to fix CO_2 (Acuña et al., 2024; Antonicelli et al., 2023; Ntagia et al., 2021). Acetyl-CoA, produced from CO_2 fixation, undergoes metabolic reactions to generate organic acids and alcohols (Sun et al., 2019). This process occurs in two phases: the acidogenic phase (organic acid production) and the solventogenic phase (conversion to alcohols). Here, CO_2 and H_2 act as electron acceptor and donor, enabling CO_2 fixation and sustainable bioproduction (Mariën et al., 2024). Despite successes in CO_2, CO, and H_2 fermentation (Doll et al., 2018; Fernández-Naveira et al., 2019; Phillips et al., 2015), research on CO_2/H_2 fermentation remains in the early stages of bioengineering. Currently, these processes are primarily producing acetate (Molitor et al., 2019) and low ethanol titers (Heffernan et al., 2020). Ongoing efforts aim to expand production to more valuable medium-chain C_4 and C_6 bio-based chemicals, which are crucial in ensuring economic viability of CO_2 fermentation (Konstantinidi et al., 2023; Thunuguntla et al., 2024).

Among clostridial acetogens, *Clostridium carboxidivorans* sp. 624 is known for producing various C_2 to C_6 acids and alcohols, such as acetate, butyrate, ethanol, butanol,

hexanoate, and hexanol, when metabolizing syngas or CO-based feedstocks (Oh et al., 2022; Phillips et al., 2015). In syngas fermentation (CO/H□/CO□ [70/20/10]), it produced ethanol (~3.0 g/L), butanol, and hexanol (0.94 g/L) (Phillips et al., 2015), while a different syngas mixture (CO/H□/CO□ [30/40/30]) led to a total alcohol yield of 4.32 g/L, with hexanol (1.90 g/L) as the dominant product (Oh et al., 2022). Despite these successes with syngas-based fermentations, studies focusing exclusively on CO□/H□ fermentation remain limited. A recent study exploring Adaptive Laboratory Evolution (ALE) techniques reported modest yields of acetate (0.82 g/L), butyrate (0.38 g/L), and hexanoate (0.40 g/L), alongside low alcohol titers (0.23 to 0.27 g/L) under CO□/H□ fermentation (Antonicelli et al., 2023). These findings highlight the challenges in CO□/H□ fermentation, such as limited metabolite titers and product distribution variability, pointing to a gap in optimizing microbial pathways and fermentation parameters for sustainable biomanufacturing. Nonetheless, CO□/H□ fermentation is crucial for sustainable bioproduction as it directly utilizes CO□, a major greenhouse gas, without requiring CO.

In addition to experimental validation, modelling and simulation play a crucial role in bioprocess optimization by enabling the analysis of multiple parameters in silico. More importantly, modelling insights reduce the need for laborious trial-and-error experimentation, thereby accelerating the overall optimization process. For C_1 gas fermentation by the clostridial microbiome, modelling not only provides a mathematical framework for microbial reactions, but also for gas-liquid mass transfer dynamics, and physiochemical gradients. Kinetic modelling captures microbial metabolic pathways and integrates dynamic mass balance models to generate time-dependent metabolite profiles. However, models specific to CO□/H□ fermentation by clostridial strains producing C□-C□ metabolites are lacking, with most studies focused on CO as the primary substrate (Ruggiero et al., 2022; Younesi et al., 2005). Computational tools, including dynamic simulations and computational fluid

dynamics (CFD), assess mass transfer, which is critical in gas-to-liquid fermentation systems (Puiman et al., 2022). Modelling CO_2 and H_2 spatial distribution helps understand their impact on microbial growth and metabolite production (Singh et al., 2024). In this study, we propose to employ an integrated kinetic modelling approach that combines experimental data to facilitate sensitivity analyses aimed at identifying key rate-limiting steps, such as acetyl-CoA utilization. This will guide the optimization of the fermentation process for C_2-C_6 acids and alcohols (Thunuguntla et al., 2024). We anticipate that this approach will enhance bioreactor design, operational strategies, and microbial consortia, ultimately leading to higher product yields (Costa et al., 2016). This advancement in CO_2/H_2-based biomanufacturing addresses gaps in microbial activity and process parameters that remain unexplored in the literature.

Herein, we systematically evaluated *C. carboxidivorans* sp. 624 for CO_2/H_2-based fermentation aimed at optimizing the production of C_2–C_6 acids and alcohols through a hybrid in-silico and experimental approach. The study begins by assessing the effects of cultivation temperature (25°C, 30°C, and 37°C) and media composition (enriched vs. minimal media) on the production of key metabolites like acetate and ethanol. With the optimal cultivation temperature identified, we conducted a time-course study to examine the dynamics of C_2–C_6 acid and alcohol production, providing insights into metabolic pathways and intermediate accumulation over time. Building on this experimental data, we developed a hybrid CFD simulation-first principles model to predict substrate utilization and product formation. This model helps validate the optimal gas-to-liquid ratio for CO_2/H_2 fermentation and offers insights into spatial inhomogeneities during the gas-liquid fermentation process. By combining kinetic modelling and CFD, we can optimize operating conditions, enhancing microbial gas fermentation and process design. Moreover, this approach demonstrates scalability, offering valuable insights for transitioning from lab-scale

to pilot-scale systems, ultimately supporting the development of efficient and sustainable CO_2-to-chemical bioprocesses for commercial applications. Overall, this study presents a framework to refine fermentation performance and study of process design parameters for CO_2/H_2 fermentation.

2. Materials and Methods

2.1 Microorganism and medium preparation

C. carboxidivorans sp. BAA-624 was purchased from American Type Culture Collection (ATCC, USA). Two types of media were used in this study: Modified PETC medium and Reinforced Clostridial Medium (RCM, Thermo Scientific™ Oxoid™ Reinforced Clostridial Medium). The modified PETC medium was prepared by dissolving the following components per liter of deionized water: 0.10 g KCl, 0.20 g $MgSO_4 \cdot 7H_2O$, 0.80 g NaCl, 0.10 g KH_2PO_4, 0.02 g $CaCl_2 \cdot 2H_2O$, 1.00 g yeast extract, and 2.00 g $NaHCO_3$. Additionally, 10 mL of modified Wolfe's metals solution (Med 1788) and 10 mL of Wolfe's vitamin solution (MD-VS; Med 1019) were added to supplement the medium. RCM was prepared from a dehydrated powder (Thermo Scientific™ Oxoid™, catalog number CM0149B) according to the manufacturer's instructions. The formulation per liter of medium included 13.00 g yeast extract, 10.00 g peptone, 1.00 g soluble starch, 5.00 g glucose, 0.50 g cysteine hydrochloride, 5.00 g sodium chloride, 3.00 g sodium acetate, and 0.50 g agar. Batch fermentation experiments

C. carboxidivorans sp. 624 cultures, in the mid-exponential growth phase, were used as the inoculum for batch fermentation experiments aimed at assessing the effects of temperature and media composition on growth and metabolite production. Fermentation was conducted in 30 mL sterilized serum bottles, each containing 15 mL of PETC/RCM medium and 15 mL of headspace. The headspace was flushed for 1 minute with a CO_2/H_2 gas

mixture (20/80), after which the pressure was equilibrated to 150 kPa (1.5 bar) with the same gas. To maintain consistent gas substrate availability, the headspace of each culture bottle was replenished daily by flushing with fresh CO□/H□ (20/80) for 1 minute and equilibrated to 150 kPa. Fermentation was carried out at 25°C, 30°C, and 37°C under mild agitation at 200 rpm using an orbital shaker (Yih Der, LM-570RD). The aim was to determine the optimal temperature for *C. carboxidivorans* sp. 624 gas fermentation by analysing the production of C□ metabolites.

Once the optimal temperature and medium were identified, subsequent fermentation experiments were conducted to expand the product range to include medium-chain metabolites (C□ and C□). Following this, a computational model (see **Section 2.4** and **2.5**) was implemented to examine the impact of different liquid-to-gas volume (V_L/V_G) ratios (0.25, 1, and 4) on the C_2-C_6 metabolites. Control cultures were prepared by sparging with N□ gas following the same procedure as the experimental conditions, which involved sparging for 1 minute and equilibrating to 150 kPa. Detailed results for N□ gas controls are presented in *Supplementary materials* (**Tables S1, S2** and **S4**). All data are reported as mean values from triplicate experiments ± standard error of the mean.

2.2 Analytical methods

Biomass analysis: The samples from fermentation were analysed with a multimode microplate reader (Thermo Scientific™ Varioskan™ LUX, USA) for optical density (OD800nm) measurements, and a correlation factor was used to obtain cell dry weight (CDW) concentrations. To obtain CDW conversion factor, a sample volume with known OD was pelletised and supernatant discarded. The pellet was dried at 60 °C for 48 hours followed by gravimetric analysis to determine CDW% per volume. Maximum specific growth rates were estimated by applying a non-linear regression to the experimentally obtained data for CDW concentrations.

Metabolites analysis: C_2-C_6 metabolites (ethanol, butanol, hexanol, acetate, butyrate, and hexanoate) from fermentation were analysed using a gas chromatography (GC) (Agilent 6890N GC, Agilent Technologies, USA) with a flame ionization detector (FID) and fused silica capillary column (DB-WAX 60 m length x 0.53 mm diameter x 1.00 µm film thickness). Helium was used as the carrier gas. The initial oven temperature was set at 35 ^{o}C with a holding time of 4 min, and then gradually increased to 220 ^{o}C at a rate of 10 ^{o}C/min, and held at the final temperature for 6 min. The injector and detector temperatures were both set to 300°C. Prior to GC analysis, the sample was centrifuged, and the supernatant was filter through a 0.22 µm filter. A 0.5 mL portion of the supernatant was then acidified with 0.02 mL of 0.6 N HCl before proceeding with the analysis.

2.3 Kinetic model of microbial reactions

The biochemical reactions involved in the conversion of CO_2/H_2 to C_2-C_6 acids and alcohols by *C. carboxidivorans* sp. 624 during both the acetogenic and solventogenic phases, via the WLP and reverse *β*-oxidation, are presented in equations below (**eq. 1-6**).

Acetogenic phase:

$$4H_2 + 2CO_2 \rightarrow CH_3COOH + 2H_2O \quad (1)$$

$$CH_3COOH + 6H_2 + 2CO_2 \rightarrow C_3H_7COOH + 4H_2O \quad (2)$$

$$C_3H_7COOH + 6H_2 + 2CO_2 \rightarrow C_5H_{11}COOH + 4H_2O \quad (3)$$

Solventogenic phase:

$$CH_3COOH + 2H_2 \rightarrow C_2H_5OH + H_2O \quad (4)$$

$$C_3H_7COOH + 2H_2 \rightarrow C_4H_9OH + H_2O \quad (5)$$

$$C_5H_{11}COOH + 4H_2 \rightarrow C_6H_{13}OH + H_2O \quad (6)$$

To describe the rates of acids production (q_{AC}, q_{BA} and q_{HA}), modified monod equations to incorporate the inhibition effects of non-substrate fatty acids were applied (**eq. 7-**

9). The conversion rate of acids in the presence of H_2 to produce alcohols (q_E, q_B and q_H) were expressed as monod kinetic for substrates (**eq. 10-12**).

$$q_{Ac} = \mu_{Ac} \frac{C_{H2}}{K^i_{H2}+C_{H2}} \frac{K_{Ac}}{K_{Ac}+C_{Ac}} \frac{K_{BA}}{K_{BA}+C_{BA}} \quad (7)$$

$$q_{BA} = \mu_{BA} \frac{C_{H2}}{K^i_{H2}+C_{H2}} \frac{C_{Ac}}{K_{Ac}+C_{Ac}} \frac{K_{BA}}{K_{BA}+C_{BA}} \quad (8)$$

$$q_{HA} = \mu_{HA} \frac{C_{H2}}{K^i_{H2}+C_{H2}} \frac{C_{BA}}{K_{BA}+C_{BA}} \frac{K_{AC}}{K_{AC}+C_{AC}} \quad (9)$$

$$q_E = \mu_E \frac{C_{H2}}{K^j_{H2}+C_{H2}} \frac{C_{UAC}}{K_{UAC}+C_{UAc}} \quad (10)$$

$$q_B = \mu_B \frac{C_{H2}}{K^j_{H2}+C_{H2}} \frac{C_{UBA}}{K_{UBA}+C_{UBA}} \quad (11)$$

$$q_H = \mu_H \frac{C_{H2}}{K^j_{H2}+C_{H2}} \frac{C_{UHA}}{K_{UHA}+C_{UHA}} \quad (12)$$

where μ_i (i=AC, BA, HA) are the maximum uptake rates of biomass for acids production, μ_j (j=E, B, H) are the maximum production rates of alcohols, K^i_{H2},K_i (i=AC, BA, HA) are affinity constants for biomass, K^j_{H2},K_m *(m=UAC, UBA, UHA)* are saturation constants of H_2, undissociated acids. C_n (n=AC, BA, HA, H2, UAC, UBA, UHA) concentration in liquid phase. (Abbreviation: AC-acetate, BA-butyrate, HA-hexanoate, E-ethanol, B-butanol, and H-hexanol)

The component mass balance equations for the gas and liquid phases are provided in *Supplementary Materials* (**Equation A1**). These first-principles 0D dynamic model equations were numerically solved to generate time profiles for product formation, and kinetic model parameters were estimated to achieve optimal representation of the experimental data. The mass transfer coefficient (K_La) and Henry's constant (K_H) for H□ were obtained from literature sources (Manna et al., 2024).

2.5 CFD simulation for gas fermentation in serum bottle

To model multiphase flows in bioreactors, the Eulerian-Eulerian solver for multiple incompressible fluid phases in OpenFOAM (Weller et al., 1998) was employed for transient simulations. This solver treats each phase as a continuous fluid with distinct volume fractions, making it suitable for modelling and analysing complex fluid interactions in scenarios such as gas-liquid-cell flows and bubbly flows. Given the critical role of mass transfer in controlled aeration and microbial metabolism, we implemented the Higbie mass transfer model to the OpenFOAM framework, which demonstrated superior accuracy compared to the existing spherical and Frossling gas-liquid mass transfer models (Mast et al., 2024). The detailed equations for this implementation were provided in **Eq. 13–16**.

In the current simulation framework, the biological model serves as a phenomenological representation of the complex metabolic processes of a specific microorganism. To enhance computational efficiency, the reaction model was simplified while retaining key kinetic phenomena necessary for quantitative experimental validation. This reduced-order model was then integrated with the multiphase flow model to capture essential biochemical interactions. The evolution of microbial and species concentrations follows the kinetic model detailed in *Supplementary Materials* (**Equation A1**). The system of ordinary differential equations governing these processes was solved using an implicit integration solver, while species transport was coupled with a second-order explicit Runge-Kutta scheme to ensure numerical stability and accuracy.

The multiphase CFD model is described as follows:

The mass conservation equation for each phase *i* is given by

$$\frac{\partial}{\partial t}(\alpha_i \rho_i) + \nabla \cdot (\alpha_i \rho_i \boldsymbol{V}_i) = 0 \tag{13}$$

and the momentum equation for each phase i is given by

$$\frac{\partial}{\partial t}(\alpha_i \rho_i \boldsymbol{V}_i) + \nabla \cdot (\alpha_i \rho_i \boldsymbol{V}_i \boldsymbol{V}_i) = -\alpha_i \nabla \mathrm{P} + \alpha_i \rho_i \boldsymbol{g} + \nabla \cdot (\alpha_i \bar{R}_i) + \boldsymbol{F}_i \qquad (14)$$

where ρ_i is the density, V_i is the phase velocity, P is the mean pressure, $\bar{R}_i$ is the combined viscous and Reynolds stresses for phase i; and F_i is the interface momentum transfer term, which is the sum of all the interfacial forces (lift, drag, virtual mass, wall lubrication, turbulent-dispersion forces, etc) acting on phase I from the other phase. It is noted that this term will influence bubble rise velocity and has large effect on gas hold-up calculation.

The transport of chemical species is modelled with passive scalar in each phase ad is given by

$$\frac{\partial}{\partial t}\left(\alpha_i \rho_i \boldsymbol{Y}_{ij}\right) + \nabla \cdot \left(\alpha_i \rho_i \boldsymbol{Y}_{ij} \boldsymbol{V}_i\right) = \nabla \cdot \left(\alpha_i \rho_i \bar{D}_{ij} \nabla Y_{ij}\right) + \dot{R}_{ij}^{MT} \qquad (15)$$

Here Y_{ij} represents the mass fraction of species j in phase i, $\bar{D}_{ij}$ is the total species diffusion coefficient including both molecular and turbulent diffusion, and $\dot{R}_{ij}^{MT}$ is the interface mass transfer term for species j in phase i.

The Higbie mass transfer equation is given by,

$$\mathrm{Sh} = 1.14\mathrm{Re}^{0.5}\mathrm{Sc}^{0.5} \qquad (16)$$

where Re is Reynold number, Sc is the Schmidt number which was used to characterize the mass diffusion and convection processes.

3. Results and Discussions

3.1 Effect of cultivation temperature and media on C_2 metabolite production

Most acetogens thrive at 20–45°C, with an optimal growth temperature around 37°C (Harahap and Ahring, 2023). Syngas fermentation at 30–37°C has been successful with *C.*

carboxidivorans sp. 624 (Oh et al., 2023, 2022; Sun et al., 2015), but recent studies explored lower temperatures (25°C) using ALE techniques to enhance gas solubility and substrate availability (Antonicelli et al., 2023). Evaluating fermentation across different temperatures can optimize process efficiency and improve biomanufacturing yields.

The growth profiles of *C. carboxidivorans* sp. 624 in both PETC and RCM media at cultivation temperatures of 25°C, 30°C, and 37°C, were investigated using a CO_2/H_2 gas substrate (20/80) at a headspace pressure of 150 kPa (*Supplementary materials*, **Fig. S1a** and **b**). The growth profiles provide an overview, indicating that cells efficiently metabolized CO_2/H_2 as a preferred substrate and reached maximal CDW within 24 hours. Following this peak, CDW values plateaued, transitioning into a gradual decline by 72 hours and continuing until 168 hours. This decline is likely attributed to substrate depletion or product inhibition from accumulated acids or alcohols, suggest a dynamic interplay between growth and metabolic byproducts in the fermentation process (Benevenuti et al., 2021).

Among the tested temperatures, lower temperature 25°C yielded the highest CDW values in both media, with RCM's rich nutrient composition boosting CDW to 0.253±0.032 g/L, while PETC media recorded at 0.038±0.001 g/L, at 24 hours. As the temperature increased to 30°C, CDW values slightly decreased (<2.6%) in both media, but showed a more pronounced drop at 37°C, showing a 13.1% reduction in PETC and 22.9% in RCM. The sharper decline in RCM is likely due to nutrient saturation, particularly sodium acetate, which promotes rapid growth but can lead to product inhibition, while PETC's minimal nutrients support slower, more stable growth. This correlation of growth with temperature also aligns with findings reported in the literature (Oh et al., 2022), where cell growth increased with decreasing cultivation temperatures.

For C metabolite production (acetate and ethanol) (*Supplementary materials*, **Fig. S1c** and **f**), the results revealed distinct effects of temperature and media on production trends. In PETC media, acetate yield peaked at 0.62 ± 0.03 g/L within the first 24 hours at 25°C, suggesting that moderately lower temperatures enhance enzymatic activity and microbial metabolism, favouring acetogenesis. As fermentation progressed, acetate concentrations plateaued and gradually declined, coinciding with a steady increase in ethanol production from 24 to 168 hours, indicating a metabolic shift from acetogenesis to solventogenesis. By 168 hours, ethanol stabilized at 0.42 ± 0.1 g/L. In contrast, RCM media at 25°C supported sustained acetate production over a longer duration, achieving a peak yield of 3.68±0.29 g/L at 168 hours, with ethanol production also peaking at 0.99±0.1 g/L by the same time, indicating a gradual transition to solventogenesis. At 30°C in RCM, acetate production was significant within the first 24 hours (3.10±0.05 g/L) but plateaued early, remaining in the range of 3.00–3.15 g/L until 168 hours, potentially due to substrate limitations or altered metabolic allocation at slightly higher temperatures. These findings suggested that lower temperatures (<37°C) favour acetate production in the initial phases, while media composition plays a critical role in sustaining production and influencing the transition to ethanol over time.

Previous research indicates that *C. carboxidivorans* sp. 624 typically exhibits optimal growth between 37-40°C (Liou et al., 2005). However, in our study, this temperature range did not yield the highest alcohol production. In contrast, this finding aligns with prior studies suggesting that lower temperatures favour ethanol production and carbon chain elongation (Ramió-Pujol et al., 2015). Lowering the temperature to 25°C appeared to have promoted the re-assimilation of organic acids and shifted metabolic pathways toward solventogenesis. The reduced temperature likely helps prevent “acid crash" where excessive acid accumulation inhibits further microbial activity, thus facilitating the conversion of acids like acetate into

alcohols. Cooler temperatures also slow down microbial growth rates, reducing the rate of acid accumulation and thereby redirecting metabolic flux from acidogenesis to solventogenesis (Shen et al., 2020). This metabolic shift explains the enhanced ethanol production observed at 25°C in our study. Additionally, the superior performance of RCM media compared to PETC can be attributed to its enriched nutrient composition, which supports higher cell densities (CDW) and more robust metabolic activity. This increased cellular activity likely contributes to higher metabolite yields, making RCM a more effective medium for maximizing both alcohol and acid production.

3.2 C_2-C_6 metabolite production at 25°C in RCM medium

Building on the findings from the temperature optimization study, which identified 25°C as the most effective temperature for metabolite production, subsequent study was conducted in RCM medium to investigate the dynamics of C_2-C_6 metabolite production. To gain a deeper understanding of the growth patterns and metabolite production, detailed sampling of C_2-C_6 metabolites was conducted at 24, 48, 72, and 120 hours. This comprehensive study not only clarified metabolic trends but also demonstrated the potential for producing medium-chain metabolites, such as C_4 and C_6 acids and alcohols, highlighting an enhancement in chain elongation.

The trend in CDW results observed in this study (**Fig. 1a**) corroborates with the findings in earlier study on cultivation temperature and media (in **Section 3.1**), where cell growth peaked at 24 hours (exponential phase) before gradually declining and eventually reaching the stationary phase on 120 hours. As for the C_2-C_6 acid metabolites, acetate (**Fig. 1b**) was the primary product during the exponential growth phase, reaching a notable concentration of 3.22±0.22 g/L in RCM at 24 hours. Acetate concentration continued to rise gradually, though not significantly, eventually reaching 4.38±0.21 g/L in RCM by the end of the experiment at 120 hours, likely due to the cells' sustained metabolic activity. The slower

rate of increase after 24 hours could be attributed to the inhibitory effects of accumulating byproducts, such as butanol, hexanoate, and hexanol (Oh et al., 2022). Similar trends for butyrate and hexanoate production were observed, where production was significant in the first 24 hours and slowed down after. Butyrate production (**Fig. 1c**) commenced during the exponential growth phase, reaching a limited concentration of 0.34±0.02 g/L within the first 24 hours. The concentration steadily increased throughout the fermentation period, peaking at 0.412±0.06 g/L by 120 hours. Hexanoate (**Fig. 1d**) exhibited a more rapid onset of production, starting at an initial concentration of 1.08±0.12 g/L at 24 hours and steadily increasing throughout the fermentation period to 1.7±0.15 g/L by 120 hours. In the absence of a CO□/H□ gas substrate, the production of hexanoate to butyrate occurs at a molar ratio of approximately 6.8:1 over 24 hours. However, when a CO□/H□ gas substrate is introduced, the hexanoate-to-butyrate ratio decreases to about 3.2:1. This shift suggests that CO□/H□ enhances butyrate production relative to hexanoate, likely due to *C. carboxidivorans* sp. 624 utilizing the supplied reducing equivalents to favour chain elongation from acetate to butyrate. The observed limitation in hexanoate accumulation may reflect a metabolic bottleneck or the depletion of reducing power required for further elongation to C_6 products. These findings emphasize the importance of optimizing electron donor-to-acceptor ratios and fermentation conditions to enhance selectivity for medium-chain fatty acids. This study aligns with the findings of Fernández-Naveira et al. (2019), who reported that hexanoate surpassed butyrate levels 24 hours after inoculation during fermentation with natural acidification (without pH control).

At this stage, ethanol emerged as the dominant solvent produced, with higher concentrations compared to butyrate and hexanol (**Fig. 1b, c,** and **d**). Specifically, ethanol reached a concentration of 0.25±0.14 g/L, while butyrate was measured at a lower concentration of 0.042±0.03 g/L, and hexanol remained undetectable within the first 24

hours. This pronounced difference suggests a preferential pathway towards ethanol production during the early solventogenesis phase. This finding aligns with a recent study that have documented ethanol production beginning early in fermentation, with maximum titers achieved within the first 20 hours (Pisacane et al., 2024).

In contrast, medium-chain alcohols such as butanol and hexanol required a significantly longer fermentation time to reach detectable levels. By 120 hours, butanol had increased to 0.082±0.02 g/L, while hexanol was still produced in very low amounts, with only 0.035±0.06 g/L detected. This delay in medium-chain alcohol production could be explained by the organism's hierarchical use of metabolic pathways, where ethanol is synthesized first to balance redox conditions, and the synthesis of longer-chain alcohols follows once energy and reducing equivalents are sufficient to drive these more complex reactions (Bae et al., 2022).

(Fig. 1)

3.3 Biokinetic model parameter estimation and experimental validation

The biokinetic model parameters, presented in *Supplementary Materials* (**Table S3**), were estimated by minimizing the root mean square error (RMSE) between predicted and experimental time-resolved metabolite concentrations. The estimated parameters include the maximum biomass uptake rate for acid production, substrate affinity constants for biomass, maximum specific production rate of alcohols, substrate saturation constants, biomass decay rate, and yield coefficients. Due to the constraints of small-scale systems (e.g., serum bottles), where limited sample volume restricts the simultaneous measurement of substrate concentrations in both gas and dissolved phases, only metabolite profiles were used for model calibration. Initial parameter estimates for chain elongation were derived from literature studies on C□–C□ acid production from CO□/H□ mixtures in membrane biofilm reactors

(Chen and Ni, 2016). The current study yielded higher C□–C□ acid concentrations than previous reports (Chen and Ni, 2016; Lanzillo et al., 2020), leading to an increased uptake rate constant and a lower affinity constant, reflecting their inverse relationship.

The calibrated biokinetic parameters indicate that the maximum uptake rates of biomass ($\mu_{AC,\ BA,\ HA}$) for acid production align with observed acid production trends in gas fermentation. Notably, the maximum uptake rate for hexanoate production exceeds that of butyrate, likely due to the greater availability of reducing equivalents from H□, which enhances reduction steps in the chain elongation pathway. Similarly, the maximum production rates of alcohols correlate well with observed alcohol titers, reinforcing the consistency of the model with experimental outcomes. Furthermore, the hydrogen affinity constant for biomass in acid production is in agreement with previously reported works (Chen and Ni, 2016).

(Fig. 2)

The time-resolved metabolite concentration profiles obtained from first-principles 0D dynamic simulations using the calibrated model parameters were presented in **Fig. 2**. The simulated profiles exhibit strong alignment with the experimental metabolite concentrations over time, capturing key phases of gas fermentation, including biomass growth and decay, as well as the acetogenesis and solventogenesis processes. The RMSE value of 0.18 quantitatively underscores the model's accuracy in predicting experimental trends, falling within the acceptable range (typically <0.3). Notably, the model successfully reproduced the maximum biomass concentration (0.25 g/L at ~24 hours) and the final titers of C□–C□ acids and alcohols at 120 hours. This agreement suggests that the kinetic framework accurately describes microbial metabolic shifts under CO□/H□ conditions. The ability to simulate both acidogenesis and solventogenesis further supports previous studies indicating that acetogens

regulate electron flow to optimize carbon flux, with H□ availability influencing the distribution of reduced products (Hermann et al., 2020; Zhu et al., 2020). Moreover, the model's predictive capability highlights the robustness of parameter estimation, ensuring reliable representation of the gas fermentation process across varying operating conditions. This is particularly relevant for process scale-up, where accurate kinetic modelling is essential for optimizing bioreactor performance and product selectivity (Singh et al., 2024).

The computational model was developed to investigate the effect of the liquid-to-gas volume ratio (V_L/V_G) on metabolite formation, providing quantitative insights into biomass growth, dissolved H□ concentration, and metabolite distribution. Simulated total acid and alcohol concentrations at 24, 48, and 72 hours revealed that increasing the liquid volume enhances metabolite production, as presented in **Fig. 3a, b** and **c**. These model predictions were further validated by experimental CO□/H□ gas fermentation studies (**Fig. 3d, e** and **f**), confirming the reliability of the computational approach. Biomass growth followed a similar trend to product formation (**Fig. S1a**), increasing with higher V_L/V_G, suggesting that larger liquid volumes improve gas solubility and substrate availability, thereby enhancing microbial metabolism. The larger liquid phase improves mass transfer rates by increasing the contact area between gas and liquid, reducing diffusion limitations (Lanzillo et al., 2020). The dissolved H□ concentration profiles showed a gradual decline over time, with the lowest concentration at $V_L/V_G = 0.25$ and the highest at $V_L/V_G = 4$ (**Fig. S2b**). This trend emphasize the importance of liquid volume in stabilizing gas uptake rates, as a larger liquid phase can buffer against rapid depletion of dissolved H□ by acting as a reservoir, thereby sustaining microbial metabolism for extended periods (Rahimi et al., 2018). Conversely, in lower V_L/V_G conditions, H□ diffusion may be insufficient to match microbial consumption rates, leading to premature depletion and suboptimal metabolic activity (Ruggiero et al., 2022). These

findings highlight the importance of gas-liquid mass transfer, where a larger liquid phase facilitates better substrate diffusion, ultimately boosting metabolic efficiency.

(**Fig. 3**)

The experimental results also showcase the considerable impact of V_L/V_G on the distribution of products, including C_2-C_6 acids and alcohols (**Fig. 4**). At 24 hours, acetate (C_2 acid) was the dominant product across all V_L/V_G conditions (0.25, 1, and 4), with the highest concentration observed at V_L/V_G = 4 (3.339 g/L), likely due to enhanced CO□ and H□ solubility promoting acetogenesis via the WLP. By 72 hours, acetate remained the primary product, but V_L/V_G = 1 (3.542 g/L) achieved the highest yield, with V_L/V_G = 4 (3.22 g/L) and V_L/V_G = 0.25 (2.85 g/L) following. Notably, longer-chain acids, including butyrate (C_4) and hexanoate (C_6), were significantly enhanced at V_L/V_G = 4 conditions, likely due to the higher H□ availability facilitating chain elongation. The enriched liquid phase in V_L/V_G = 4 conditions likely improved gas diffusion and substrate bioavailability, fostering more efficient microbial metabolism (Tharak and Venkata Mohan, 2024). Additionally, excess H□ drives the reduction of acids into alcohols, as observed in ethanol (0.317 g/L), butanol (0.061 g/L), and hexanol (0.033 g/L) production at 72 hours. The interaction between gas and liquid phases enhances mass transfer, increasing the availability of reducing equivalents that shift metabolic flux toward alcohol synthesis (Bae et al., 2022).

(Fig. 4)

Comparisons with CO-based fermentation suggest that electron donor availability strongly influences product distribution. CO fermentation typically yields higher butyrate due to electron limitations, whereas CO□/H□ fermentation, with abundant reducing power, shifts metabolic preference toward hexanoate after acetate (Lanzillo et al., 2020; Mariën et al.,

2024). Unsurprisingly, the total acids and alcohols, as well as the acid-to-alcohol ratio, were strongly influenced by the H_2/CO_2 feedstock ratio (80:20) and the WLP (**Fig. 3d, e** and **f**). At 72 hours, V_L/V_G = 4 conditions yielded the highest total acids (5.341 g/L) and alcohols (0.411 g/L), highlighting the role of an H_2-rich environment in enhancing acetogenesis and chain elongation. The lower acid-to-alcohol ratio (13.00) at V_L/V_G = 4 conditions indicates higher acid conversion to alcohols, supporting product diversification through excess hydrogenation. Conversely, at V_L/V_G = 1, the fermentation produced the highest acid-to-alcohol ratio (17.93), favouring acetate production as moderate H_2 availability promoted acetogenesis while minimizing solventogenesis.

Collectively, these findings demonstrate the interplay between gas-liquid interactions, substrate availability, and metabolic pathways in CO_2/H_2 fermentation. The computational model provides predictive insights that align with experimental observations, reinforcing the significance of optimizing V_L/V_G and electron donor-to-acceptor ratios to tailor product distribution in CO_2-based bioprocesses.

3.4 CFD simulations

A detailed understanding of the nonuniform spatial distributions of key components, such as substrates and metabolites, is crucial as these factors significantly influence cell growth and final bioproduction yields. To capture both temporal variations and spatial distributions within the bioreactor, the biokinetic model and estimated parameters were further integrated with computational fluid dynamics (CFD) simulations. The concentration contours of the biomass and acetate from 3D CFD simulations of the serum bottle model were analyzed at various time points (5, 18, and 72 hours) during the CO_2/H_2 conversion process by *Clostridium carboxidivorans* sp. 624 (**Fig. 5a**). The simulations revealed that biomass concentrations increased progressively from 5 to 18 hours, reflecting an active

metabolic phase marked by rapid cell proliferation. However, a significant decrease in biomass concentration was predicted at 72 hours. This finding aligns with experimental data, which showed a decline in biomass after 24 hours, indicating a transition to the decay phase, likely due to substrate depletion and the accumulation of inhibitory metabolites.

Simulated acetate concentrations exhibit a continuous increase from 5 to 72 hours (**Fig. 5b**). Although acetate is subsequently converted into ethanol, its sustained accumulation suggests its role as a key intermediate during the fermentation process. Notably, the spatial distribution patterns of biomass and acetate closely resemble each other, reinforcing the interdependence of microbial growth and metabolite production during acetogenesis. This strong correlation suggests that acetate biosynthesis is tightly linked to microbial proliferation, where active cell metabolism facilitates continuous acetate generation (Kurt et al., 2023).

(Fig. 5)

At 5 hours, acids predominate while alcohol levels remain negligible, indicating the early acetogenic phase in the time-resolved concentration profiles (**Fig. 5c**). By 18 hours, acids accumulate significantly more than alcohols, confirming the dominance of acetogenesis over solventogenesis. At 72 hours, both acids and alcohols reach their maximum concentrations, reflecting the transition into solventogenesis as reducing equivalents become more available for alcohol formation (**Fig. 5d**). The temporal distinction between these metabolic phases is consistent with previous studies on syngas fermentation, where an extended acetogenic phase is followed by solventogenesis under excess H□ conditions (Lanzillo et al., 2020).

Additionally, comparing the time-resolved concentration profiles of biomass and metabolites further demonstrates a strong qualitative and quantitative agreement between first

principles-based estimations and CFD simulations (**Fig. 6**). In small-scale batch systems, such as the serum bottle model, spatial variations and convective mixing effects are minimal, leading to a close match between 0D dynamic models and CFD simulations. However, in continuous stirred-tank reactors (CSTRs), where physical and mechanical non-uniformities become more pronounced, greater discrepancies between CFD and first-principles-based predictions are expected (Hanspal et al., 2023). This underscores the critical role of CFD simulations in scaling up gas fermentation processes, where spatial heterogeneities in substrate distribution, gas-liquid mass transfer, and hydrodynamics significantly impact bioprocess efficiency. In larger bioreactors, factors such as mixing intensity, bubble dynamics, and localized nutrient gradients can lead to non-uniform microbial activity, potentially limiting productivity (Singh et al., 2024). Future studies will extend these simulations to pilot-scale systems, enabling a deeper understanding of fluid flow behaviour, optimizing gas-to-liquid transfer efficiency, and refining operational strategies for enhanced metabolite yields in industrial applications.

(Fig. 6)

3.5 Comparison studies

To contextualize the current results, the production of C_2-C_6 metabolites by *C. carboxidivorans* sp. 624 was compared with previous literature (**Table 1**). Studies on syngas (CO, CO□, H□, N□) fermentation using this strain have reported varied titers of acids and alcohols under differing gas compositions, pressures, and media. While direct comparisons are challenging, due to the diversity in experimental setups, common trends and limitations can be identified.

In this study, acetate was the predominant product, achieving a significant concentration of 4.38 g/L, while butyrate and hexanoate reached moderate levels of 0.41 g/L

and 1.70 g/L, respectively. Ethanol production, at 0.29 g/L, was consistent with the limited alcohol yields commonly observed in syngas fermentation, attributed to the low-energy yields of acetogen metabolism (Ciliberti et al., 2020). These findings align with studies showing lower alcohol production relative to acids. For example, (Ramió-Pujol et al., 2015) reported ethanol titers of 3.97 g/L under elevated pressure (200 kPa) and with the addition of morpholinoethanesulfonic acid (MES), which may enhance solventogenesis. Most studies, including this one, utilized batch reactors, which are constrained by limited gas-liquid mass transfer due to the low solubility of gaseous substrates (CO□ and H□) in water. Although trace metal supplementation improved metabolite yields in other studies (Phillips et al., 2015), the limitations of batch fermentation underscore the need for continuous systems to enhance productivity. Such systems can optimize gas transfer and stabilize fermentation conditions, potentially increasing alcohol yields (Asimakopoulos et al., 2018). The comparison highlights the importance of reactor design improvements and genetic modifications to boost solvent production efficiency.

Further insight into the metabolic pathways underlying C_2-C_6 production can be gained from the WLP, central to the metabolism of *C. carboxidivorans* sp. 624 (Fernández-Blanco et al., 2023; Stark et al., 2022; Thunuguntla et al., 2024). This pathway converts CO□ into acetyl-CoA, a key intermediate for synthesizing both acids and alcohols. Acetyl-CoA can be further elongated into butyryl-CoA and hexanoyl-CoA, leading to the formation of medium-chain acids (butyrate, hexanoate) and alcohols (butanol, hexanol). The strain's ability to utilize this pathway enables efficient conversion of CO□ and H□ into a range of C_2-C_6 products. H□ plays a pivotal role in this process as an electron donor, driving the reduction of CO□ through key enzymatic reactions (Takors et al., 2018). Sufficient H□ availability not only ensures optimal redox balance but also enhances microbial growth and metabolic activity, resulting in higher production rates of target metabolites (Konstantinidi et al., 2023).

In this study, the delay in medium-chain alcohol production suggests a metabolic hierarchy, where C_2 metabolites are prioritized initially to mitigate acid stress before shifting to longer-chain products.

(Table 1) Comparison of C□–C□ metabolite production by *C. carboxidivorans* sp. 624 with literature-reported values, all conducted in serum bottle-scale fermentation.

4. Conclusion

This study employed a hybrid *in-silico* and experimental approach to analyse *Clostridium carboxidivorans* sp. 624 under CO□/H□ fermentation. Batch fermentation at 25°C yielded the highest reported acetate concentration (4.38 g/L), highlighting temperature the crucial role in acetogenesis. Furthermore, systematic evaluation of the liquid-to-gas volume ratio (V_L/V_G) revealed pronounced effects on product distribution, with $V_L/V_G = 1$ maximizing acetate and $V_L/V_G = 4$ enhancing longer-chain acid synthesis due to improved gas solubility and substrate availability. The enriched liquid phase at $V_L/V_G = 4$ also increased total acid (5.341 g/L) and alcohol (0.411 g/L) yields, favouring solventogenesis. By integrating an unstructured kinetic model with 3D CFD simulations, we unveiled valuable insights into gas-liquid interactions and temporal-spatial distributions of the metabolites. Looking ahead, future research will continue to refine bioreactor design, optimise gas-phase parameters, and leverage strain engineering to enhance yields and product distribution, paving the way for the development of scalable CO□ bioconversion technologies aimed at carbon-negative biomanufacturing.

CRediT authorship contribution statement

Yong Wei Tiong: Writing – original draft, Methodology, Investigation, Formal analysis, Data curation, Conceptualization.

Ashriel Yong: Writing – review & editing, Methodology, Investigation, Formal analysis, Data curation, Conceptualization.

Anjaiah Nalaparaju: Writing – review & editing, Methodology, Investigation, Formal analysis, Data curation, Conceptualization

Hoang-Huy Nguyen: Writing – review & editing, Methodology, Investigation, Formal analysis, Data curation, Conceptualization

Li Quan Koh: Writing – review & editing, Validation.

Roong Jien Wong: Writing – review & editing, Validation.

Ron Tau Yee Lim: Writing – review & editing, Validation.

Dave Siak-Wei Ow: Writing – review & editing, Validation, Supervision.

Jia Zhang: Writing – review & editing, Validation, Resources.

Van Bo Nguyen: Writing – review & editing, Validation, Resources.

Fong Tian Wong: Writing – review & editing, Validation, Supervision, Project administration, Methodology, Funding acquisition, Conceptualization, Resources.

Yee Hwee Lim: Writing – review & editing, Validation, Supervision, Project administration, Methodology, Funding acquisition, Conceptualization, Resources.

Declaration of competing interest

The authors declare that they have no known competing financial interests or personal relationships that could have appeared to influence the work reported in this paper.

Acknowledgements

The authors gratefully acknowledge financial support from Agency for Science, Technology and Research (A*STAR), Singapore (C233017002 and Singapore Integrative Biosystems and Engineering Research Strategic Research & Translational Thrust (SIBER SRTT). The computational work for this article was partially performed on resources of the National Supercomputing Centre (NSCC), Singapore (https://www.nscc.sg).

References

Acuña, P., Rebecchi, S., Vlaeminck, E., Quataert, K., Frilund, C., Laatikainen-luntama, J., Hiltunen, I., Winter, K. De, Soetaert, W.K., 2024. Demonstrating Pilot-Scale Gas Fermentation for Acetate Production from Biomass-Derived Syngas Streams. Fermentation 10, 1–13.

Antonicelli, G., Ricci, L., Tarraran, L., Fraterrigo Garofalo, S., Re, A., Vasile, N.S., Verga, F., Pirri, C.F., Menin, B., Agostino, V., 2023. Expanding the product portfolio of carbon dioxide and hydrogen-based gas fermentation with an evolved strain of Clostridium carboxidivorans. Bioresource Technology 387. https://doi.org/10.1016/j.biortech.2023.129689

Asimakopoulos, K., Gavala, H.N., Skiadas, I. V., 2018. Reactor systems for syngas fermentation processes: A review. Chemical Engineering Journal 348, 732–744. https://doi.org/10.1016/j.cej.2018.05.003

Bae, J., Song, Y., Lee, H., Shin, J., Jin, S., Kang, S., Cho, B.K., 2022. Valorization of C1 gases to value-added chemicals using acetogenic biocatalysts. Chemical Engineering Journal 428, 131325. https://doi.org/10.1016/j.cej.2021.131325

Benevenuti, C., Branco, M., Do Nascimento-Correa, M., Botelho, A., Ferreira, T., Amaral, P., 2021. Residual gas for ethanol production by clostridium carboxidivorans in a dual impeller stirred tank bioreactor (Stbr). Fermentation 7. https://doi.org/10.3390/fermentation7030199

Chen, X., Ni, B.J., 2016. Anaerobic conversion of hydrogen and carbon dioxide to fatty acids production in a membrane biofilm reactor: A modeling approach. Chemical Engineering Journal 306, 1092–1098. https://doi.org/10.1016/j.cej.2016.08.049

Ciliberti, C., Biundo, A., Albergo, R., Agrimi, G., Braccio, G., de Bari, I., Pisano, I., 2020. Syngas derived from lignocellulosic biomass gasification as an alternative resource for innovative bioprocesses. Processes 8, 1–38. https://doi.org/10.3390/pr8121567

Costa, R.S., Hartmann, A., Vinga, S., 2016. Kinetic modeling of cell metabolism for microbial production. Journal of Biotechnology 219, 126–141. https://doi.org/10.1016/j.jbiotec.2015.12.023

Doll, K., Rückel, A., Kämpf, P., Wende, M., Weuster-Botz, D., 2018. Two stirred-tank bioreactors in series enable continuous production of alcohols from carbon monoxide with Clostridium carboxidivorans. Bioprocess and Biosystems Engineering 41, 1403–1416. https://doi.org/10.1007/s00449-018-1969-1

Dziejarski, B., Krzyżyńska, R., Andersson, K., 2023. Current status of carbon capture, utilization, and storage technologies in the global economy: A survey of technical assessment. Fuel 342. https://doi.org/10.1016/j.fuel.2023.127776

Fernández-Blanco, C., Robles-Iglesias, R., Naveira-Pazos, C., Veiga, M.C., Kennes, C., 2023. Production of biofuels from C1-gases with Clostridium and related bacteria—Recent advances. Microbial Biotechnology. https://doi.org/10.1111/1751-7915.14220

Fernández-Naveira, Á., Veiga, M.C., Kennes, C., 2019. Selective anaerobic fermentation of syngas into either C2-C6 organic acids or ethanol and higher alcohols. Bioresource Technology 280, 387–395. https://doi.org/10.1016/j.biortech.2019.02.018

Hanspal, N., DeVincentis, B., Thomas, J.A., 2023. Modeling multiphase fluid flow, mass transfer, and chemical reactions in bioreactors using large-eddy simulation. Engineering in Life Sciences 23, 1–15. https://doi.org/10.1002/elsc.202200020

Harahap, B.M., Ahring, B.K., 2023. Acetate Production from Syngas Produced from

Lignocellulosic Biomass Materials along with Gaseous Fermentation of the Syngas: A Review. Microorganisms 11. https://doi.org/10.3390/microorganisms11040995

Heffernan, J.K., Valgepea, K., de Souza Pinto Lemgruber, R., Casini, I., Plan, M., Tappel, R., Simpson, S.D., Köpke, M., Nielsen, L.K., Marcellin, E., 2020. Enhancing CO2-Valorization Using Clostridium autoethanogenum for Sustainable Fuel and Chemicals Production. Frontiers in Bioengineering and Biotechnology 8, 1–10. https://doi.org/10.3389/fbioe.2020.00204

Hermann, M., Teleki, A., Weitz, S., Niess, A., Freund, A., Bengelsdorf, F.R., Takors, R., 2020. Electron availability in CO2, CO and H2 mixtures constrains flux distribution, energy management and product formation in Clostridium ljungdahlii. Microbial Biotechnology 13, 1831–1846. https://doi.org/10.1111/1751-7915.13625

Konstantinidi, S., Skiadas, I. V., Gavala, H.N., 2023. Microbial Enrichment Techniques on Syngas and CO2 Targeting Production of Higher Acids and Alcohols. Molecules 28. https://doi.org/10.3390/molecules28062562

Kurt, E., Qin, J., Williams, A., Zhao, Y., Xie, D., 2023. Perspectives for Using CO2 as a Feedstock for Biomanufacturing of Fuels and Chemicals. Bioengineering 10, 1–41. https://doi.org/10.3390/bioengineering10121357

Lanzillo, F., Ruggiero, G., Raganati, F., Russo, M.E., Marzocchella, A., 2020. Batch syngas fermentation by clostridium carboxidivorans for production of acids and alcohols. Processes 8, 1–13. https://doi.org/10.3390/pr8091075

Lau, H.C., Ramakrishna, S., Zhang, K., Shahul Hameed, M.Z., 2021. A Decarbonization Roadmap for Singapore and Its Energy Policy Implications. Energies 14, 1–23. https://doi.org/10.3390/su14148425

Liew, F.M., Martin, M.E., Tappel, R.C., Heijstra, B.D., Mihalcea, C., Köpke, M., 2016. Gas Fermentation-A flexible platform for commercial scale production of low-carbon-fuels and chemicals from waste and renewable feedstocks. Frontiers in Microbiology 7. https://doi.org/10.3389/fmicb.2016.00694

Liou, J.S.C., Balkwill, D.L., Drake, G.R., Tanner, R.S., 2005. Clostridium carboxidivorans sp. nov., a solvent-producing clostridium isolated from an agricultural settling lagoon, and reclassification of the acetogen Clostridium scatologenes strain SL1 as Clostridium drakei sp. nov. International Journal of Systematic and Evolutionary Microbiology 55, 2085–2091. https://doi.org/10.1099/ijs.0.63482-0

Manna, D., Chowdhury, R., Calay, R.K., Mustafa, M.Y., 2024. Experimental Insights into the Fermentation of Pyro-Syngas to Ethanol in a Semi-Batch and Continuous Stirred Bioreactor with Mathematical Modelling and Optimization. Energies 17. https://doi.org/10.3390/en17030562

Mariën, Q., Flores-Alsina, X., Aslam, U., Gernaey, K. V., Regueira, A., Ganigué, R., 2024. Isobutyric and n-butyric acid production from H2 and CO2 by Clostridium luticellarii in a hollow fiber membrane biofilm reactor: Reactor operation and process modelling. Chemical Engineering Journal. https://doi.org/10.1016/j.cej.2024.153216

Mast, Y., Wild, M., Takors, R., 2024. Optimizing Mass Transfer in Multiphase Fermentation: The Role of Drag Models and Physical Conditions. Processes 12. https://doi.org/10.3390/pr12010045

Molitor, B., Mishra, A., Angenent, L.T., 2019. Power-to-protein: Converting renewable electric power and carbon dioxide into single cell protein with a two-stage bioprocess. Energy and Environmental Science 12, 3515–3521. https://doi.org/10.1039/c9ee02381j

Ntagia, E., Chatzigiannidou, I., Carvajal-Arroyo, J.M., Arends, J.B.A., Rabaey, K., 2021.

Continuous H2/CO2 fermentation for acetic acid production under transient and continuous sulfide inhibition. Chemosphere 285. https://doi.org/10.1016/j.chemosphere.2021.131536

Oh, H.J., Gong, G., Ahn, J.H., Ko, J.K., Lee, S.M., Um, Y., 2023. Effective hexanol production from carbon monoxide using extractive fermentation with Clostridium carboxidivorans P7. Bioresource Technology 367, 1–9. https://doi.org/10.1016/j.biortech.2022.128201

Oh, H.J., Ko, J.K., Gong, G., Lee, S.M., Um, Y., 2022. Production of Hexanol as the Main Product Through Syngas Fermentation by Clostridium carboxidivorans P7. Frontiers in Bioengineering and Biotechnology 10, 1–11. https://doi.org/10.3389/fbioe.2022.850370

Phillips, J.R., Atiyeh, H.K., Tanner, R.S., Torres, J.R., Saxena, J., Wilkins, M.R., Huhnke, R.L., 2015. Butanol and hexanol production in Clostridium carboxidivorans syngas fermentation: Medium development and culture techniques. Bioresource Technology 190, 114–121. https://doi.org/10.1016/j.biortech.2015.04.043

Pisacane, S., Lanzillo, F., Raganati, F., Marzocchella, A., 2024. Production of Alcohols from C1-waste Gas Fermentation by Clostridium Carboxidivorans in a Continuous Gas Fed Bioreactor. Chemical Engineering Transactions 110, 181–186. https://doi.org/10.3303/CET24110031

Puiman, L., Abrahamson, B., Lans, R.G.J.M. va. der, Haringa, C., Noorman, H.J., Picioreanu, C., 2022. Alleviating mass transfer limitations in industrial external-loop syngas-to-ethanol fermentation. Chemical Engineering Science 259, 117770. https://doi.org/10.1016/j.ces.2022.117770

Raganati, F., Ammendola, P., 2024. CO2 Post-combustion Capture: A Critical Review of Current Technologies and Future Directions. Energy and Fuels.

https://doi.org/10.1021/acs.energyfuels.4c02513

Rahimi, M.J., Sitaraman, H., Humbird, D., Stickel, J.J., 2018. Computational fluid dynamics study of full-scale aerobic bioreactors: Evaluation of gas–liquid mass transfer, oxygen uptake, and dynamic oxygen distribution. Chemical Engineering Research and Design 139, 283–295. https://doi.org/10.1016/j.cherd.2018.08.033

Ramió-Pujol, S., Ganigué, R., Bañeras, L., Colprim, J., 2015. Incubation at 25°C prevents acid crash and enhances alcohol production in Clostridium carboxidivorans P7. Bioresource Technology 192, 296–303. https://doi.org/10.1016/j.biortech.2015.05.077

Ricci, L., Agostino, V., Fino, D., Re, A., 2021. Screening of gas substrate and medium effects on 2,3-butanediol production with C. Ljungdahlii and C. autoethanogenum aided by improved autotrophic cultivation technique. Fermentation 7. https://doi.org/10.3390/fermentation7040264

Ruggiero, G., Lanzillo, F., Raganati, F., Russo, M.E., Salatino, P., Marzocchella, A., 2022. Bioreactor modelling for syngas fermentation: Kinetic characterization. Food and Bioproducts Processing 134, 1–18. https://doi.org/10.1016/j.fbp.2022.04.002

Singh, V.K., Jiménez del Val, I., Glassey, J., Kavousi, F., 2024. Integration Approaches to Model Bioreactor Hydrodynamics and Cellular Kinetics for Advancing Bioprocess Optimisation. Bioengineering 11, 1–17. https://doi.org/10.3390/bioengineering11060546

Stark, C., Münßinger, S., Rosenau, F., Eikmanns, B.J., Schwentner, A., 2022. The Potential of Sequential Fermentations in Converting C1 Substrates to Higher-Value Products. Frontiers in Microbiology 13. https://doi.org/10.3389/fmicb.2022.907577

Sun, L., Pope, P.B., Eijsink, V.G.H., Schnürer, A., 2015. Characterization of microbial community structure during continuous anaerobic digestion of straw and cow manure.

Microbial Biotechnology 8, 815–827. https://doi.org/10.1111/1751-7915.12298

Sun, X., Atiyeh, H.K., Huhnke, R.L., Tanner, R.S., 2019. Syngas fermentation process development for production of biofuels and chemicals: A review. Bioresource Technology Reports. https://doi.org/10.1016/j.biteb.2019.100279

Takors, R., Kopf, M., Mampel, J., Bluemke, W., Blombach, B., Eikmanns, B., Bengelsdorf, F.R., Weuster-Botz, D., Dürre, P., 2018. Using gas mixtures of CO, CO2 and H2 as microbial substrates: the do's and don'ts of successful technology transfer from laboratory to production scale. Microbial Biotechnology 11, 606–625. https://doi.org/10.1111/1751-7915.13270

Tharak, A., Venkata Mohan, S., 2024. Electrode-Assisted Pressurized CO2 Fermentation for Acetic Acid and Ethanol Production: Enhanced Carbon Fixation, Metabolic Efficiency, and Sustainability in Carbon-Negative Bioprocesses. ACS Sustainable Chemistry and Engineering 13, 352–373. https://doi.org/10.1021/acssuschemeng.4c07537

Thunuguntla, R., Atiyeh, H.K., Huhnke, R.L., Tanner, R.S., 2024. CO2-based production of C2-C6 acids and alcohols: The potential of novel Clostridia. Bioresource Technology Reports 25. https://doi.org/10.1016/j.biteb.2023.101713

Ulpiani, G., Vetters, N., Melica, G., Bertoldi, P., 2023. Towards the first cohort of climate-neutral cities: Expected impact, current gaps, and next steps to take to establish evidence-based zero-emission urban futures. Sustainable Cities and Society 95, 104572. https://doi.org/10.1016/j.scs.2023.104572

Weller, H.G., Tabor, G., Jasak, H., Fureby, C., 1998. A tensorial approach to computational continuum mechanics using object-oriented techniques. Computers in Physics 12, 620–631. https://doi.org/10.1063/1.168744

Younesi, H., Najafpour, G., Mohamed, A.R., 2005. Ethanol and acetate production from synthesis gas via fermentation processes using anaerobic bacterium, Clostridium ljungdahlii. Biochemical Engineering Journal 27, 110–119. https://doi.org/10.1016/j.bej.2005.08.015

Zhu, H.F., Liu, Z.Y., Zhou, X., Yi, J.H., Lun, Z.M., Wang, S.N., Tang, W.Z., Li, F.L., 2020. Energy Conservation and Carbon Flux Distribution During Fermentation of CO or H2/CO2 by Clostridium ljungdahlii. Frontiers in Microbiology 11. https://doi.org/10.3389/fmicb.2020.00416

Figures

Fig. 1. Results analysis of gas fermentation experiment with *C. carboxidivorans* sp. 624 in RCM medium at 25°C: **(a)** Cell growth; Production of **(b)** C_2 metabolites, **(c)** C_4 metabolites, and **(d)** C_6 metabolites. Refer to *Supplementary Materials* (**Table S2**) for N□-sparged data.

Fig. 2. Model predicted time-resolved profiles of bioconversion products along with experimental data: **(a)** biomass, **(b)** acetate, **(c)** butyrate/hexanoate, and **(d)** C_2-C_6 alcohols.

Fig. 3. Total acids and total alcohols concentrations, and also ratio of total acids to alcohols at different timing based on: Simulation **(a)** 24 hours, **(b)** 48 hours, and **(c)** 72 hours, as well as Experimental **(d)** 24 hours, **(e)** 48 hours, and **(f)** 72 hours, of gas fermentation experiment with *C. carboxidivorans* sp. 624 in RCM medium at 25°C.

Fig. 4. Results analysis of gas fermentation experiment with *C. carboxidivorans* sp. 624 in RCM medium at 25°C, with different liquid-to-gas volume ratio: **(a)** Cell growth; Production of metabolite concentration at **(b)** V_L/V_G=0.25, **(c)** V_L/V_G=1, and (d) V_L/V_G=4. Refer to *Supplementary Materials* (**Table S4**) for N□-sparged data.

Fig. 5. Concentration contours at different time points of reaction **(a)** biomass, and **(b)** acetate, **(c)** total acids, and **(d)** total alcohols.

Fig. 6. Concentration profiles calculated from first-principles dynamic model and CFD simulations, **(a)** biomass and acetate, and **(b)** total acids and total alcohols.

Fig. 1

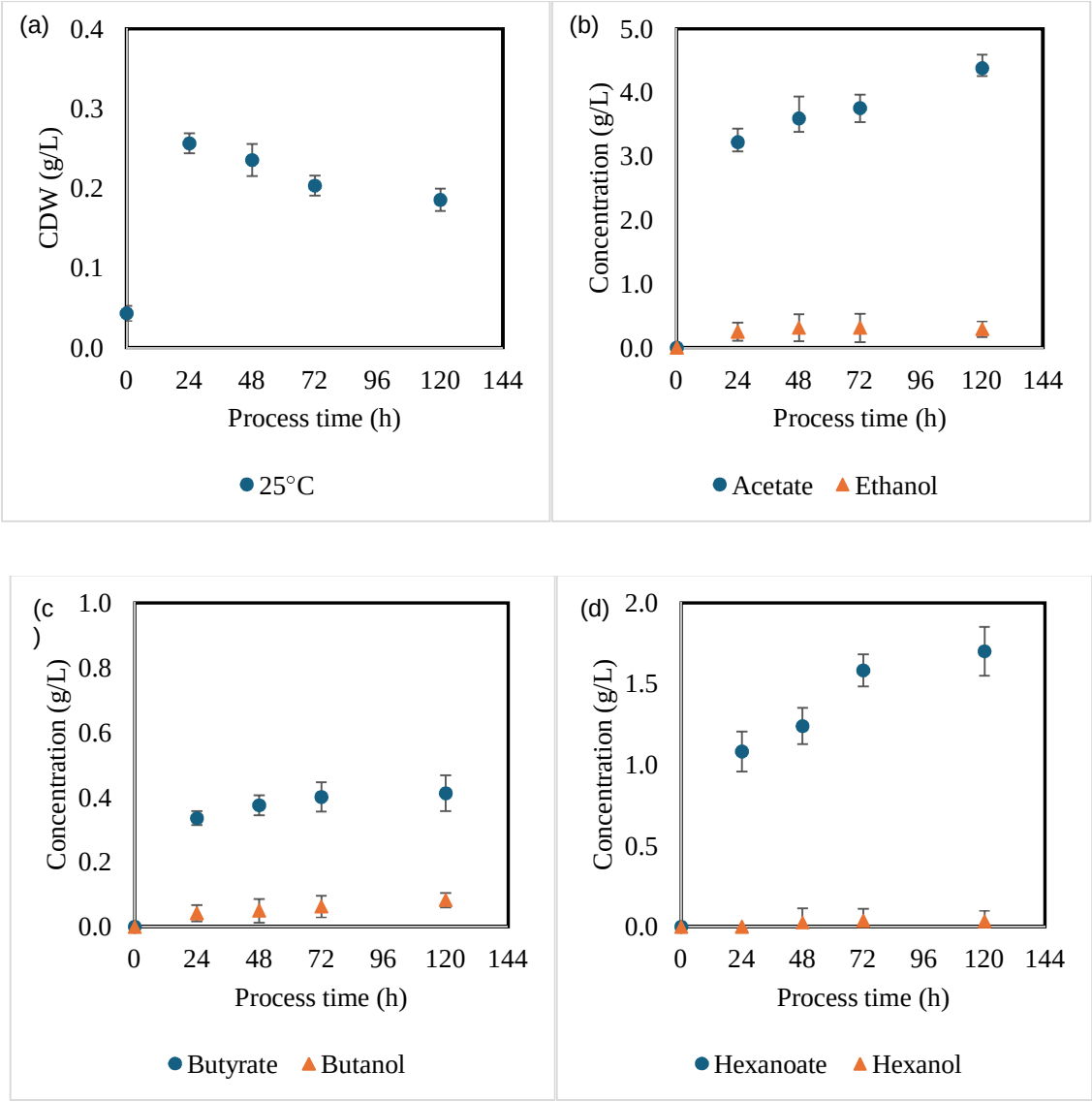
(a)
CDW (g/L)
0.4
0.3
0.2
0.1
0.0
0
24
48
72
96
120
144
Process time (h)
25°C
(b)
Concentration (g/L)
5.0
4.0
3.0
2.0
1.0
0.0
Process time (h)
Acetate
Ethanol
(c)
Concentration (g/L)
1.0
0.8
0.6
0.4
0.2
0.0
Process time (h)
Butyrate
Butanol
(d)
Concentration (g/L)
2.0
1.5
1.0
0.5
0.0
Process time (h)
Hexanoate
Hexanol

Fig. 2

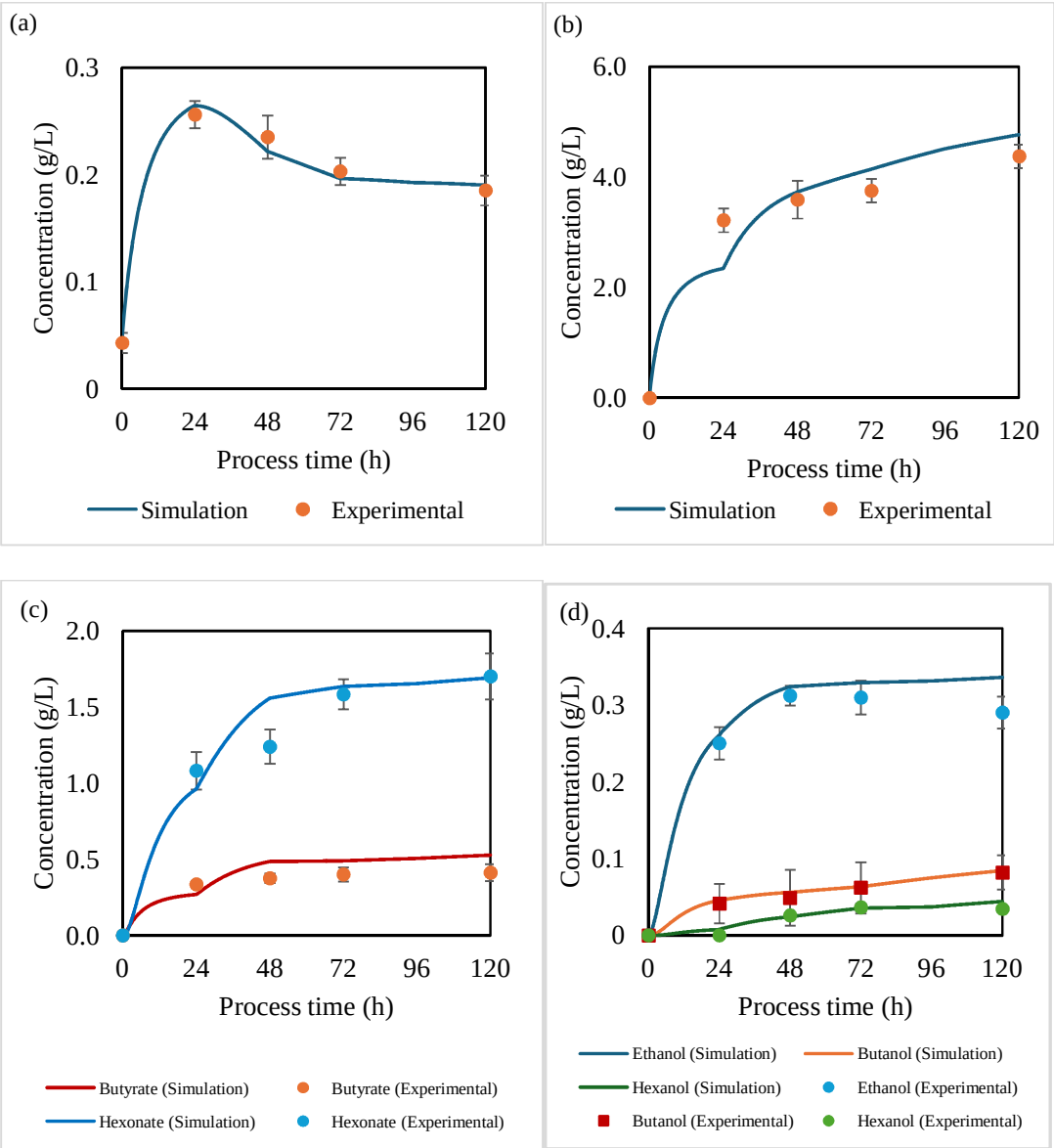
(a)
0.3
0.2
0.1
0
Concentration (g/L)
0
24
48
72
96
120
Process time (h)
Simulation
Experimental
(b)
6.0
4.0
2.0
0.0
Concentration (g/L)
0
24
48
72
96
120
Process time (h)
Simulation
Experimental
(c)
2.0
1.5
1.0
0.5
0.0
Concentration (g/L)
0
24
48
72
96
120
Process time (h)
Butyrate (Simulation)
Butyrate (Experimental)
Hexonate (Simulation)
Hexonate (Experimental)
(d)
0.4
0.3
0.2
0.1
0
Concentration (g/L)
0
24
48
72
96
120
Process time (h)
Ethanol (Simulation)
Butanol (Simulation)
Hexanol (Simulation)
Ethanol (Experimental)
Butanol (Experimental)
Hexanol (Experimental)

Fig. 3

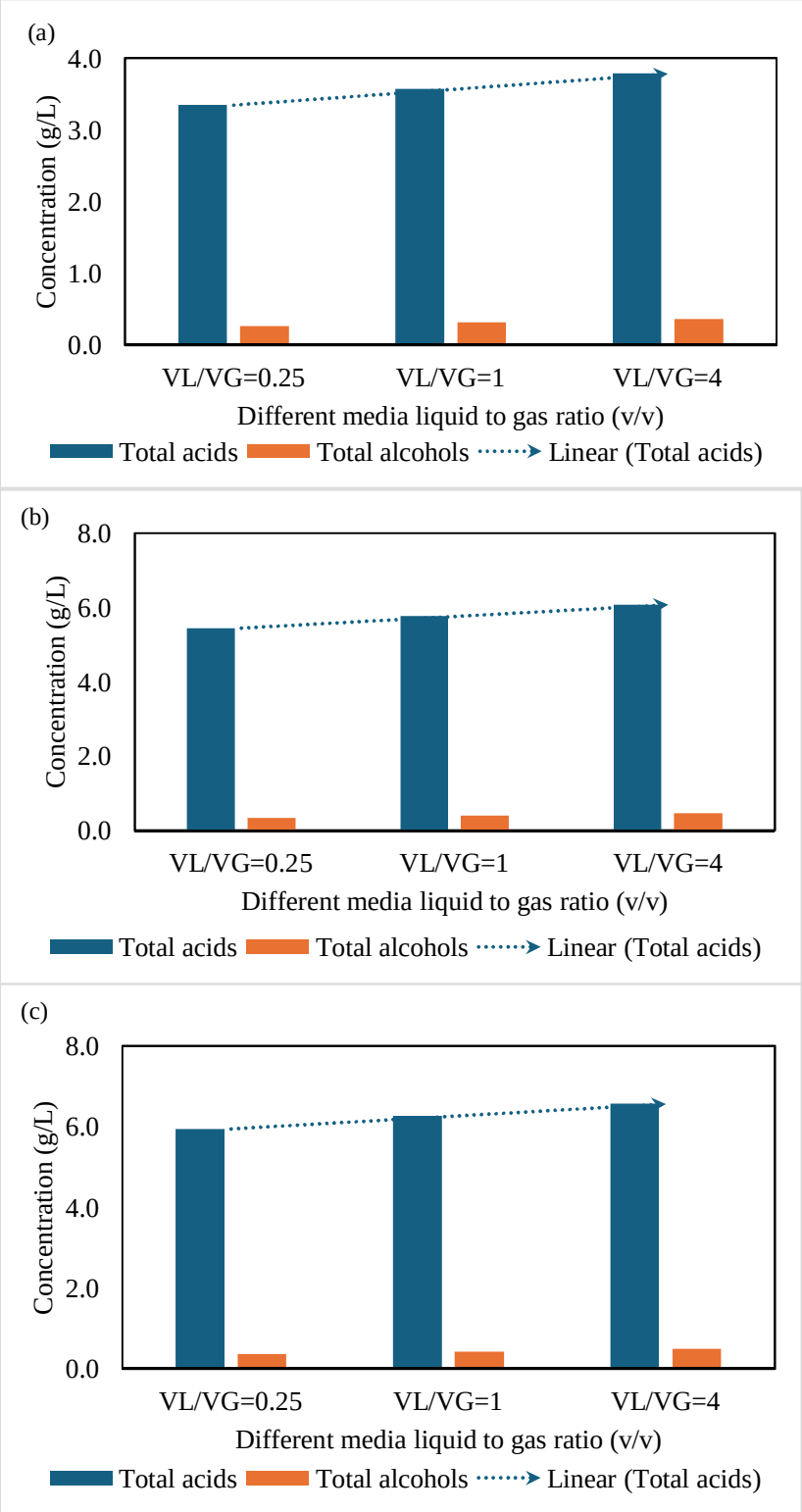
(a)
4.0
3.0
2.0
1.0
0.0
Concentration (g/L)
VL/VG=0.25
VL/VG=1
VL/VG=4
Different media liquid to gas ratio (v/v)
Total acids
Total alcohols
Linear (Total acids)
(b)
8.0
6.0
4.0
2.0
0.0
Concentration (g/L)
VL/VG=0.25
VL/VG=1
VL/VG=4
Different media liquid to gas ratio (v/v)
Total acids
Total alcohols
Linear (Total acids)
(c)
8.0
6.0
4.0
2.0
0.0
Concentration (g/L)
VL/VG=0.25
VL/VG=1
VL/VG=4
Different media liquid to gas ratio (v/v)
Total acids
Total alcohols
Linear (Total acids)

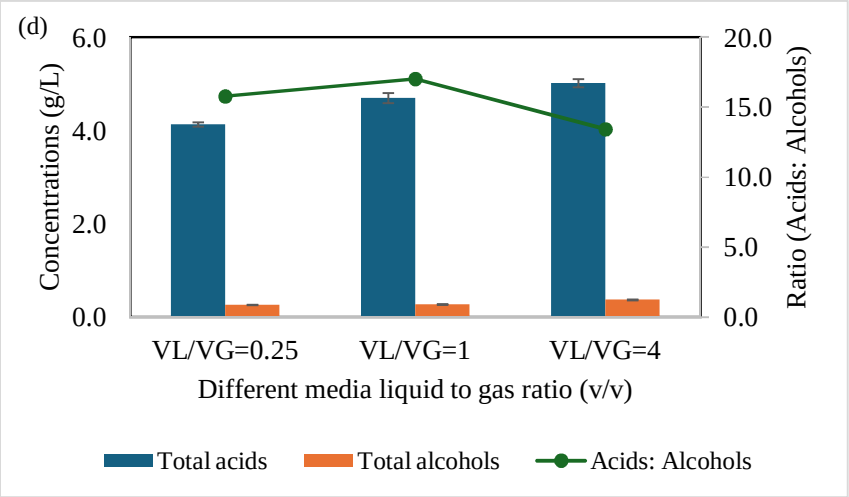
(d)
6.0
4.0
2.0
0.0
Concentrations (g/L)
20.0
15.0
10.0
5.0
0.0
Ratio (Acids: Alcohols)
VL/VG=0.25
VL/VG=1
VL/VG=4
Different media liquid to gas ratio (v/v)
Total acids
Total alcohols
Acids: Alcohols

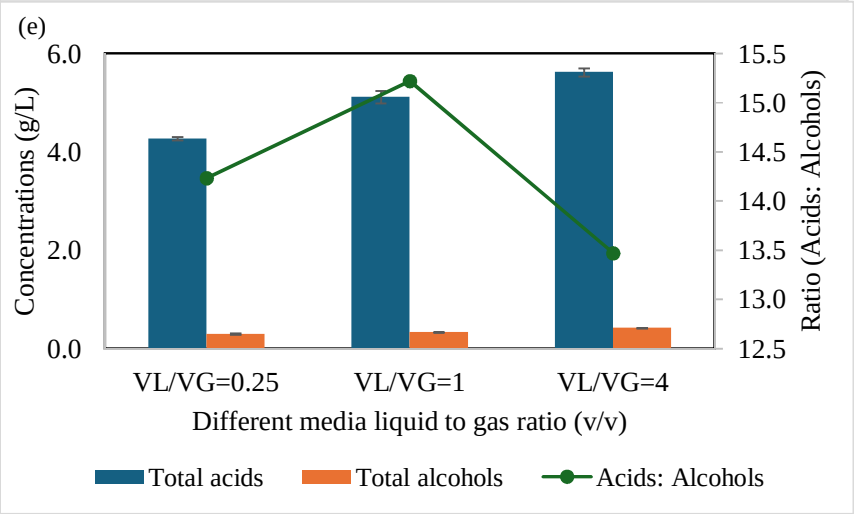
(e)
6.0
4.0
2.0
0.0
Concentrations (g/L)
15.5
15.0
14.5
14.0
13.5
13.0
12.5
Ratio (Acids: Alcohols)
VL/VG=0.25
VL/VG=1
VL/VG=4
Different media liquid to gas ratio (v/v)
Total acids
Total alcohols
Acids: Alcohols

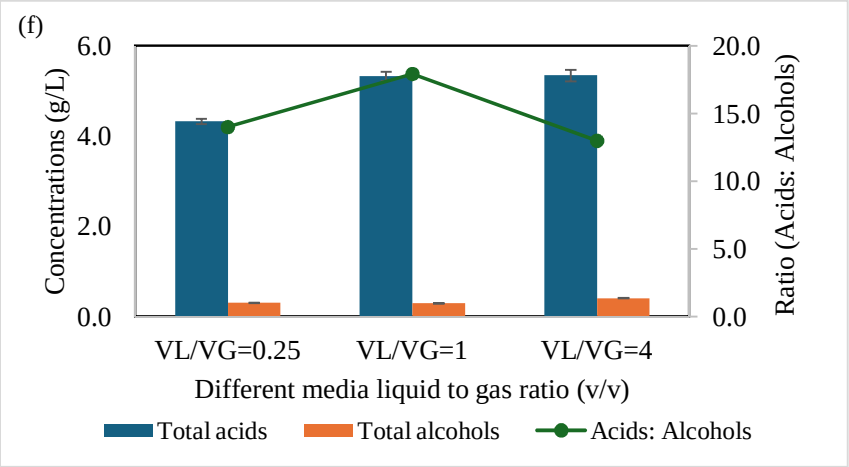
(f)
6.0
4.0
2.0
0.0
Concentrations (g/L)
20.0
15.0
10.0
5.0
0.0
Ratio (Acids: Alcohols)
VL/VG=0.25
VL/VG=1
VL/VG=4
Different media liquid to gas ratio (v/v)
Total acids
Total alcohols
Acids: Alcohols

Fig. 4

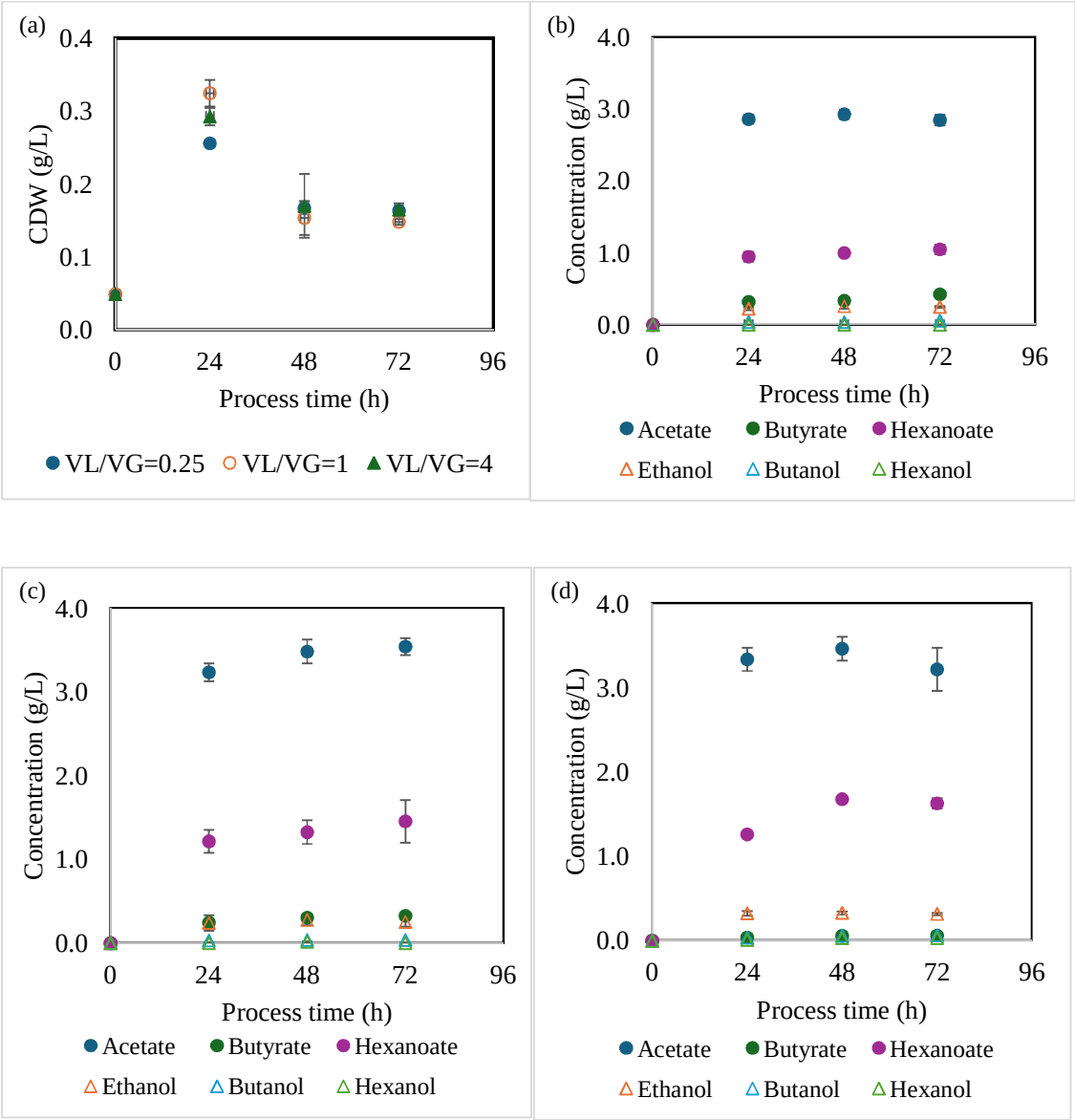
(a)
CDW (g/L)
0.4
0.3
0.2
0.1
0.0
0
24
48
72
96
Process time (h)
VL/VG=0.25
VL/VG=1
VL/VG=4
(b)
Concentration (g/L)
4.0
3.0
2.0
1.0
0.0
0
24
48
72
96
Process time (h)
Acetate
Butyrate
Hexanoate
Ethanol
Butanol
Hexanol
(c)
Concentration (g/L)
4.0
3.0
2.0
1.0
0.0
0
24
48
72
96
Process time (h)
Acetate
Butyrate
Hexanoate
Ethanol
Butanol
Hexanol
(d)
Concentration (g/L)
4.0
3.0
2.0
1.0
0.0
0
24
48
72
96
Process time (h)
Acetate
Butyrate
Hexanoate
Ethanol
Butanol
Hexanol

Fig. 5

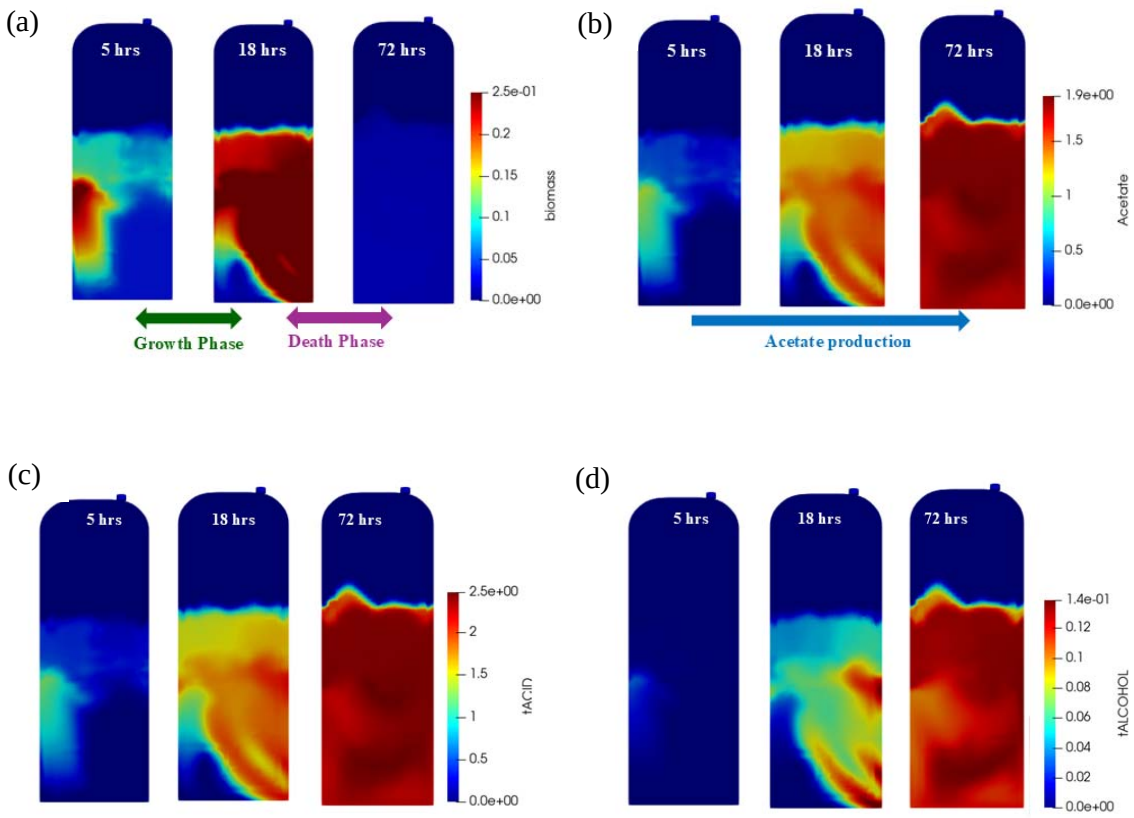
(a)
5 hrs
18 hrs
72 hrs
2.5e-01
0.2
0.15
0.1
0.05
0.0e+00
biomass
Growth Phase
Death Phase
(b)
5 hrs
18 hrs
72 hrs
1.9e+00
1.5
1
0.5
0.0e+00
Acetate
Acetate production
(c)
5 hrs
18 hrs
72 hrs
2.5e+00
2
1.5
1
0.5
0.0e+00
tACIID
(d)
5 hrs
18 hrs
72 hrs
1.4e-01
0.12
0.1
0.08
0.06
0.04
0.02
0.0e+00
tALCOHOL

Fig. 6

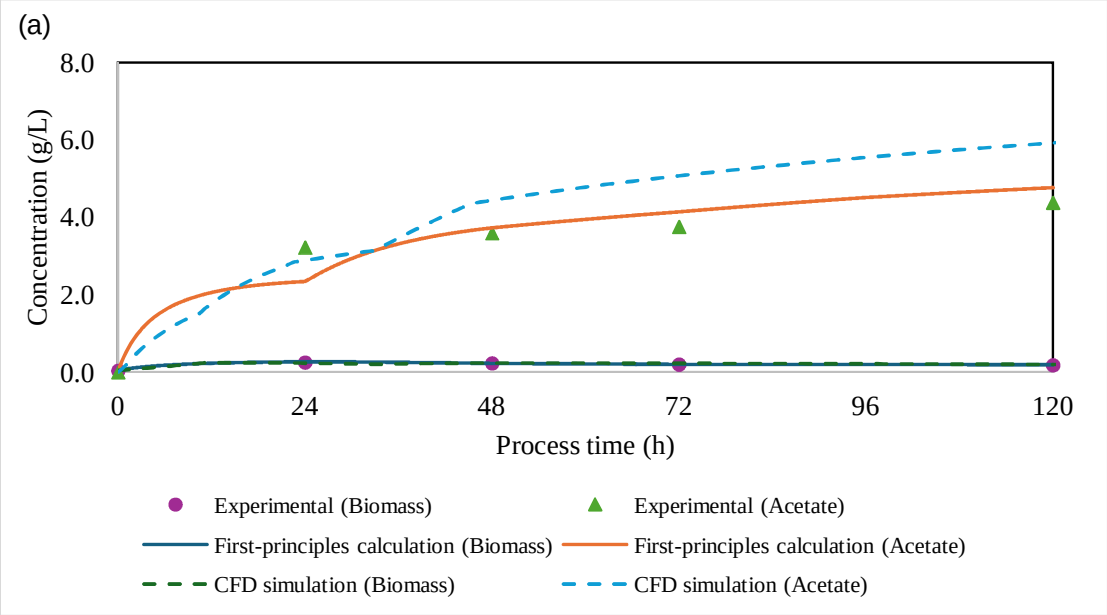
(a)
8.0
6.0
4.0
2.0
0.0
Concentration (g/L)
0
24
48
72
96
120
Process time (h)
Experimental (Biomass)
Experimental (Acetate)
First-principles calculation (Biomass)
First-principles calculation (Acetate)
CFD simulation (Biomass)
CFD simulation (Acetate)

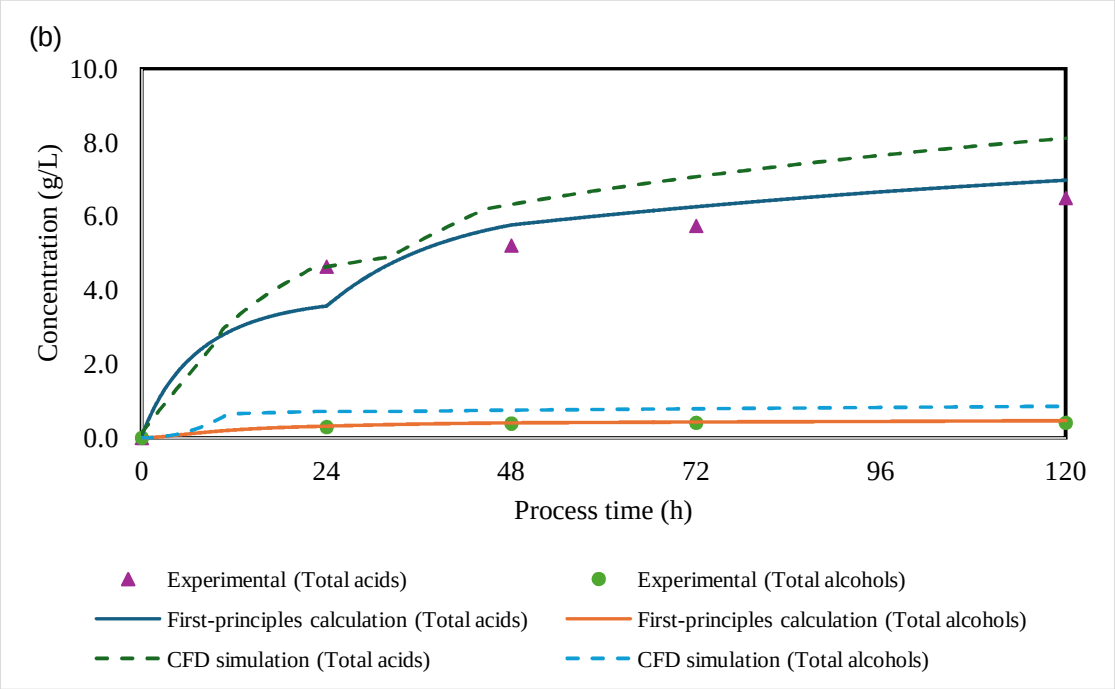
(b)
10.0
8.0
6.0
4.0
2.0
0.0
Concentration (g/L)
0
24
48
72
96
120
Process time (h)
Experimental (Total acids)
Experimental (Total alcohols)
First-principles calculation (Total acids)
First-principles calculation (Total alcohols)
CFD simulation (Total acids)
CFD simulation (Total alcohols)